

A LOFAR radio search for Crab-like pulsars in Andromeda

Joeri van Leeuwen^{1*}, Klim Mikhailov^{2,1}, Evan Keane³, Jason Hessels^{1,2}, Vlad Kondratiev^{1,4}, Daniele Michilli^{2,1}, Sotiris Sanidas^{5,2}, Ben Stappers⁵, and other contributors, potentially including LOFAR PWG⁶

¹ ASTRON, the Netherlands Institute for Radio Astronomy, Postbus 2, 7990 AA, Dwingeloo, The Netherlands

² Anton Pannekoek Institute for Astronomy, University of Amsterdam, Science Park 904, 1098 XH Amsterdam, The Netherlands

³ SKA Organisation, Jodrell Bank Observatory, Lower Withington, Macclesfield, Cheshire SK11 9DL, UK

⁴ Astro Space Center of the Lebedev Physical Institute, Profsoyuznaya str. 84/32, Moscow 117997, Russia

⁵ Jodrell Bank Center for Astrophysics, School of Physics and Astronomy, University of Manchester, Manchester M13 9PL, UK

⁶ <http://www.astron.nl/lofarpwg/>

Received ...; accepted ...

ABSTRACT

We observe bright, short bursts of radio emission from sources over a large range of distances: from the nearby Crab pulsar to remote Fast Radio Bursts (FRBs). FRBs are likely to originate from distant neutron stars, but our knowledge of the radio pulsar population has been limited to the Galaxy and the Magellanic Clouds. In an attempt to increase our understanding of extragalactic pulsar populations, and its giant-pulse emission, we employed the world's largest low-frequency radio telescope, LOFAR, to search Andromeda (M31) for radio bursts emitted by young, Crab-like pulsars. For direct comparison we also present a LOFAR study on the low-frequency giant pulses from the Crab pulsar; their fluence distribution follows a power law with slope 2.89 ± 0.02 . We confirmed the pulsar that [Rubio-Herrera et al. \(2013\)](#) reported at dispersion measure 54.7 pc cm^{-3} . A number of further candidates signals were detected from M31 but none proved persistent. FRBs are sometimes thought of as Crab-like pulsars with exceedingly bright giant pulses – given our sensitivity, we can rule out that M31 hosts pulsars more than an order of magnitude brighter than the Crab pulsar, that follow FRB-like scattering.

Key words. pulsars: general – pulsars:individual:B0531+21 – giant pulses – Galaxies: individual: M31

1. Introduction

In the 50 years since their discovery, millisecond-duration radio signals have helped map out an ever increasing volume of our Universe. Already in the first pulsar, [Hewish et al. \(1968\)](#) recognized the swept pulse delay as interstellar dispersion commensurate with a distance of $\sim 65 \text{ pc}$. Within 20 years the units grew to kpc; [McConnell et al. \(1991\)](#) detected pulsar J0045–7319 in the Small Magellanic Cloud, at 60 kpc. Finally, in the last decade, Fast Radio Bursts (FRBs) are detected that traveled many Mpc (cf. FRB121102 at luminosity distance 972 Mpc, [Tendulkar et al. 2017](#)) and even Gpc (cf. FRB160102 at $\sim 16 \text{ Gpc}$, [Bhandari et al. 2018](#)). Dispersion studies using pulsars chart out the densities in our Galaxy, while for FRBs these start to map the Universe.

Yet, a gap remains around the 1 Mpc mark. Targeted observations of our neighboring galaxy M31, at $785 \pm 25 \text{ kpc}$ ([McConnachie et al. 2005](#)), may provide insights into the pulsar or FRB population at those distances. Potential benefits of a search of M31 are its proximity; its direction well away from the Galactic plane; and its own inclination $> 10^\circ$ away from edge-on, suggesting modest dispersion measure (DM) contributions to most lines of sight. Less favorable is that its present-day star formation rate is only about half that of the Milky Way ([Yin et al. 2009](#)).

Further to measuring electron densities, extragalactic pulsar detections could sample the intergalactic magnetic field; reveal the most luminous part of the extragalactic population; and enable pulsar populations comparisons between galaxies. For these reasons nearby galaxies were previously searched for

fast transients (see [Mikhailov & van Leeuwen 2016](#), and references therein). None were successful; but for M31, [Rubio-Herrera et al. \(2013\)](#) carried out a Westerbork Synthesis Radio Telescope (WSRT) search at 328 MHz, and discovered six bursts at the same DM of 54.7 pc cm^{-3} . To firmly associate the source with Andromeda, its DM would need to exceed the foreground Galactic and intergalactic medium (IGM) dispersive smearing. Using an IGM density of $n_{\text{IGM}}=0.16 \text{ m}^{-3}$ ([Yao et al. 2017](#)) the intergalactic medium between the Milky Way and M31 would contribute only 0.13 pc cm^{-3} . That component does not significantly influence the total. The [Yao et al. \(2017\)](#) Galactic electron density model predicts the maximum Milky Way contribution in this line of sight to be $\sim 60 \text{ pc cm}^{-3}$. The uncertainties in such models, especially at high Galactic latitudes, can exceed a factor of 2 ([Deller et al. 2019](#)). Thus the source may be at the outer edge of the Milky Way, or the outer edge of M31. Following it up was a major motivation for the work presented in this paper.

We here report on this M31 search, using LOFAR ([van Haarlem et al. 2013](#)). Especially useful are the high LOFAR sensitivity; and the observing frequency of 150 MHz, where the pulsar flux density peaks ([Stappers et al. 2011](#)) and giant-pulse spectra remain steep ([Karuppusamy et al. 2012](#)). For such extragalactic LOFAR searches, M31 is the highest ranked candidate listed in [van Leeuwen & Stappers \(2010\)](#). We compare the Andromeda single-pulse results against the most powerful Galactic giant-pulse emitter, the Crab pulsar¹.

¹ The comparison additionally fitting given the mythological struggle involving Andromeda and the Sea Monster as told by [Ovidius \(8\)](#).

* E-mail: leeuwen@astron.nl

In Sect. 2 we describe the observations and data analysis; in Sect. 3, the search results and M31 rate calculations. In Sect. 4 we contrast the required M31 pulsar flux density distributions to that of the Crab pulsar. We discuss these results and conclude in Sect. 5 and 6. For all these, further background and detail is available in the corresponding Sections of Ch. 4 of [Mikhailov 2018](#) (henceforth [M18](#)).

2. Observations and data analysis

The two observations, carried out in 2011 (for 1 h) and 2014 (for 4 h) used the High Band Antennas (HBAs) of the central LOFAR “superterp”. Its high filling factor allows for coherent surveying at the highest possible speed ([Stappers et al. 2011](#); [Cohen et al. 2014](#)). While the observations are detailed in full in [Mikhailov \(2018\)](#), their main characteristics include the use of a pointing grid of around 100 tied-array beams that covers M31, M32 and M110 (Fig. 1); a central frequency around 150 MHz, and bandwidth of 29 and 78 MHz respectively; plus a ~ 1 ms sampling time and 12 kHz spectral resolution. Data were beamformed, cleaned from basic radio frequency interference (RFI), processed into 8-bit Stokes-I filterbank data using the standard LOFAR pulsar pipeline ([Alexov et al. 2010](#)) and stored in the LOFAR long term archive (LTA², [Renting & Holties 2011](#)).

Data were next dedispersed over a range of trial DMs, determined using the PRESTO ([Ransom 2001](#)) dedispersion plan optimizer. The average Galactic DM contribution towards M31 is ~ 60 pc cm⁻³, with a foreground gradient over our beam pattern of about ~ 7 pc cm⁻³, increasing toward lower galactic latitude. The inclination of M31 limits its own dispersion: DMs of order several hundreds pc cm⁻³ are expected (cf. Sect. 5.2).

The 2011 observations were thus searched up to 1000 pc cm⁻³, in 30,000 trials with increasing spacing of 0.01–0.1 pc cm⁻³. For our observing setup, the intra-channel dispersion smearing for DM=1000 pc cm⁻³ is about 30 ms ([Mikhailov 2018](#)), and for higher DMs the signal to noise of narrow bursts decreases further. Following the discovery of high-DM FRBs, the 2014 data were searched up to 2500 pc cm⁻³, in 45,000 trials. For limited computing time we retain sensitivity to very bright high-DM events there, caused by uncertainties in the DM contributions of the intergalactic medium and M31 itself, or from background FRBs unrelated to M31 (cf. FRB131104; [Ravi et al. 2015](#)). As FRBs have been detected down to 400 MHz ([CHIME/FRB Collaboration et al. 2019](#)), a detection at LOFAR frequencies could be possible, and would inform us further on the FRB emission properties.

The 2011 data was initially searched for single-pulse emission on the Hydra cluster in Manchester. Data were transferred there from the LTA over a bandwidth-on-demand 1–10 Gbps network. Search output data was partially inspected.

All 2011 and 2014 data were transferred to the Dutch national supercomputer Cartesius³. There, we performed dedispersion, periodicity and single-pulse searches using PRESTO ([Ransom 2001](#)), over the course of about 325,000 core-hours of Cartesius compute time⁴. All *periodic* candidates from slow ($P > 20$ ms) pulsar candidates with PRESTO-reported reduced $\chi^2 > 2$ were inspected by eye. We also inspected all *single-pulse* candidates of pulse width $W < 100$ ms and signal-to-noise (S/N) level over 10σ .

3. Search results

3.1. 2011 Observations

The DM = 54.7 pc cm⁻³ bursts identified in [Rubio-Herrera et al. \(2013\)](#) were recorded in a wide-field WSRT mode called 8gr8. This created 8 tied array beams, each offset within the grating response of the linear WSRT array. That allows for searches over the full field of view of the primary beams of the 25-m dish. The method could only localize this intermittent source to several bands on the sky, as shown in blue in Fig. 1, and reports the two most likely regions at RA = 11.62°; Dec = +41.44°, and at RA = 11.19°; Dec = +41.69°. While in our 2011 setup these two fall in beam 21 or 68, many other medium- to high likelihood locations fall in other beams.

In the initial pass through the RFI-free first 1000 seconds of the data on the Hydra cluster in Manchester, an excess of pulses at DM = 54.7 pc cm⁻³ was seen in beam 2, close to the prime positions (Fig. 2). These ~ 8 individual pulses appear to confirm the candidate pulsar, with a different telescope at a different frequency. The best position for the source is (RA, Dec) = (00h 44m 09s, +41° 17′) and so hereafter we refer to it as PSR J0044+4117. It was not detected in another beam. No underlying period could be detected from these 8 pulses.

All data were next blindly searched more fully on the Dutch supercomputer Cartesius. We used the LOTAAS single-pulse search pipeline⁵ ([Sanidas et al. 2019](#)) around PRESTO to remove RFI and identify individual pulses up to widths of 100 ms. Periodicity searches were carried out as detailed in [Mikhailov \(2018\)](#). We inspected the single-pulse and periodic output both by eye, and with the LOTAAS single-pulse ([Michilli et al. 2018](#)) and periodic ([Lyon et al. 2016](#)) machine-learning classifier.

Using this RFI cleaning and pipeline, the DM=54.7 pc cm⁻³ bursts were not seen as prominently as in the initial search. Some noteworthy periodic candidates were identified, but none were seen again in the 2014 observations.

3.2. 2014 Observations

A similar blind search through the 2014 data found no convincing pulsar signals from M31, M32 or M110. A close inspection of even low-significance single-pulse detections around DM=54.7 pc cm⁻³ could not reconfirm PSR J0044+4117.

We derive the LOFAR upper limits following from these non-detections using the radiometer-equation based method described in §3.2 of [Kondratiev et al. \(2016\)](#) and detailed in [Mikhailov \(2018\)](#). Our sky noise estimate includes the continuum contribution from M31 itself. We assume a 10% pulse duty cycle. For the periodicity search (ps) our estimated sensitivity $S_{\min, ps}$ reached in the full 4 hours, for a S/N = 10σ event, is 1.3 ± 0.7 mJy.

We derive the single-pulse search flux limit using Eq. 3 from [Mikhailov & van Leeuwen \(2016\)](#). For a short single pulse of width $w = 1$ ms, the minimum detectable flux density $S_{\min, sps}$ is 15 ± 8 Jy. Our minimum detectable *fluence* for a pulse of width w is thus $F_{\min}(w) = 15 \sqrt{\frac{w}{1\text{ms}}}$ Jy ms.

² Project data is public at <https://lta.lofar.eu/>

³ <https://userinfo.surfsara.nl/systems/cartesius>

⁴ <http://www.nwo.nl/onderzoek-en-resultaten/onderzoeksprojecten/i/98/26598.html>

⁵ <https://www.nwo.nl/en/research-and-results/research-projects/i/08/26608.html>

4. Comparison of giant pulses from the Crab pulsar to the M31 search

Given this sensitivity, could we detect bright giant pulses (GPs) from young neutron stars in Andromeda? To determine this, we compare against the brightest known specimen, the Crab pulsar. Below we derive the its LOFAR fluence distributions, and extrapolate to determine the odds of detecting bright, super-giant pulses (Cordes 2004; Cordes & Wasserman 2016) from M31.

4.1. The Crab pulsar at LOFAR frequencies

Earlier multi-frequency studies of Crab GPs spanned the radio spectrum from 20 MHz with LWA to 9 GHz with Arecibo (detailed in Mikhailov 2018). The 430 MHz Arecibo Crab observations by McLaughlin & Cordes (2003) suggest one GP/hr could be seen out to 1 Mpc. M31 is that close, but is out of Arecibo declination range.

To determine if LOFAR could detected Crab-like GPs from M31, we used it to observe the Crab pulsar⁶. The setup was similar to Sect. 2, but with 21 Core Stations, in “Complex Voltage” mode (Stappers et al. 2011) and coherent dedispersion with CDMT (Bassa et al. 2017a).

We flux calibrated the data following Bilous et al. (2016). The contribution from the nebula to the station-beam noise is included through the Haslam et al. (1982) 408 MHz map. Furthermore, as our tied-array beam covers $\sim 1/4$ th of the Crab Nebula, we add $1/4$ th of $S_{\text{Crab}} \approx 955 \text{ Jy} \frac{\nu}{1 \text{ GHz}}^{-0.27}$ (Bietenholz et al. 1997) to the background noise budget.

Using this approach, we determine the peak flux density and fluence of the all single pulses in our hour of data. Over a downsampling range of 5–500 ms, we identified 4000 pulses whose pulse-integrated S/N ratios exceeded 5σ (a fluence of $\sim 250 \text{ Jy ms}$). Figure 3 shows an example of the occurrence of multiple pulses within a 1-second window.

The GP fluence distribution between our lower limit of 250 Jy ms , and the brightest detected pulse of $1.1 \times 10^4 \text{ Jy ms}$, is shown in Fig. 4. The main feature of a power-law fit to its slope is the index, $\alpha = 2.89 \pm 0.02$. We note this is the fit to the differential energy distribution (as plotted in Fig. 4) not to the cumulative distribution that is equally often reported in the literature. Thus, $\alpha = 2.89 \pm 0.02$ describes the slope of the probability density function $p(F) \propto F^{-\alpha}$ as in Karuppusamy et al. (2012), not for the index we shall here call β , which describes the probability distribution $P(F > F_0) \propto F_0^{-\beta}$ as in Sallmen et al. (1999); the relation between the two is that $\beta = \alpha - 1 = 1.89$.

4.2. GPs in M31

Using this distribution, we determine whether we could have detected 1-ms wide Crab-like GPs from M31.

For such a pulsar, our minimum detectable fluence $F_{\text{min}} = S w = 15 \text{ Jy ms}$. The faintest possible detectable GP from M31 would have to be $F_{\text{Crab, M31}} = F_{\text{min}} \times (D_{\text{M31}}/D_{\text{Crab}})^2 \sim 2.3 \times 10^6 \text{ Jy ms}$ if as close as the Crab. Extrapolating the Fig. 4 1-hr histogram suggests that the 4 hr used toward M31 the fluence $F_{\text{Crab, 4hr}}$ of brightest detected pulse would be around $1.1 \times 10^4 \times 4^{1/2.89} = 1.8 \times 10^4 \text{ Jy ms}$. That is about $100\times$ dimmer than our limiting minimum sensitivity from M31.

Yet, the scattering medium to M31 is much thinner, over a longer path, than to the Crab pulsar. This means intrinsically short-duration Crab-like GPs ($5 \mu\text{s}$ in Sallmen et al. 1999) from M31 could possibly invoke little scattering. This is seen over even longer distances in FRBs (cf. Fig. 5 of Cordes et al. 2016). If we assume an average DM for sources in M31 of 150 pc cm^{-3} (cf. Sect. 5.2), this FRB relation suggests a scattering time of $\sim 10^{-5} \text{ ms}$ at 1 GHz. If we scale as $\nu^{-3.5}$, the scattering time at LOFAR frequencies is around $10 \mu\text{s}$. For such a pulsar to have been detected, its $10\text{-}\mu\text{s}$ GP from M31 would have to exceed that of the Crab by a factor $F_{\text{Crab, M31}}/F_{\text{Crab, 4hr}} \times \sqrt{0.01 \text{ ms}/1 \text{ ms}} = 13$. Our non-detection thus tells us there are no pulsars in M31 beamed at Earth that follow scattering similar to FRBs, and whose GPs are an order of magnitude brighter than those seen in the Crab Pulsar.

5. Discussion

5.1. Neutron-star formation in M31

The total star formation rate (SFR) of M31 has been stable over the last few tens of Myr, at $\sim 1 M_{\odot} \text{ yr}^{-1}$ (Williams 2003). That is roughly 2 times lower than the SFR in our Milky Way, of $1.9 \pm 0.4 M_{\odot} \text{ yr}^{-1}$ (Chomiuk & Povich 2011). The SFR is important as it maps linearly to neutron star birth rate (cf. Eq. 6 in Keane & Kramer 2008).

The neutron-star low-mass X-ray binaries (e.g., Stiele et al. 2011; Pastor-Marazuela et al. 2019) and X-ray pulsars (Esposito et al. 2016; Rodríguez Castillo et al. 2018) in M31 clearly evidence the presence of neutron stars in Andromeda. Further support is provided by its supernova remnants (SNRs). In our Galaxy, 295 are known (Green 2014). A similar number, 156, is identified in M31 (Lee & Lee 2014). Overall, the radio pulsar population in M31 may be somewhat smaller than our Milky Way, but other neutron-star detections clear suggest active pulsars are present.

5.2. Dispersion measure contributions from M31

The electron content of M31 may contribute significantly to the pulse dispersion, reducing detectability especially for sources located on its far side. To investigate the scale of this effect, we modified the Yao et al. (2017) electron-density model⁷ for our Galaxy, to describe M31. In our own Galaxy both Earth and pulsars are embedded inside the medium. M31 is observed from outside, and we aim to estimate the dispersion smearing to its mid plane. This integration over the full line of sight means the exact value of the electron density and disk scale height by themselves do not strongly influence the outcome. From the M31 mass and major-axis length, we derive the densities and scale heights. We model the gaseous disk using an electron density that doubles from the center out to a radius of 12 kpc and then falls off with a hyperbolic secant squared $\text{sech}^2(x)$ scale length of 8 kpc (Chemin et al. 2009). From this and the orientation of Andromeda in the sky we determine the dispersion measure over our survey field toward sources in the M31 mid plane (Fig. 5). The Galactic foreground of $\sim 60 \text{ pc cm}^{-3}$ covers the entire field. In around 20% of the field we expect twice that. In 10% the expected DM $> 180 \text{ pc cm}^{-3}$. All modeled dispersion measures fall within the search space. The intra-channel smearing for the highest DM ($> 180 \text{ pc cm}^{-3}$) region is 5 ms, of order 2 samples in the

⁶ Data publicly available under account at the LTA: https://lta.lofar.eu/Lofar?project=ALL&mode=query_result_page&product=UnspecifiedDataProduct&pipeline_object_id=EE400E4EC5D1358CE043C416A9C36F15

⁷ v1.3.2, http://119.78.162.254/dmodel/ymw16_v1.3.2.tar.gz

2011 data and 10 samples in the 2014 data. That is sufficiently low to suggest the deleterious effects of the M31 dispersion are limited, and not a reason for our non-detections.

5.3. Future LOFAR work

Designing a future LOFAR campaign that reaches the required 13-fold increase in sensitivity is challenging. A factor of 4 could be attained by coherently adding all 24 LOFAR core stations. An order of magnitude more tied-array beams would have to be searches, but these could be preferentially positioned on the M31 disk to regain observing efficiency.

If the high flux-density tail of the distribution is described by the same power law as as found in our 1 h observation (Fig. 4), the remaining factor of 3 could be overcome through an observing campaign $3^{2.89}$ times longer than our current 4 hr, i.e., 100 hr. These results strongly depend on the yet unknown super-giant pulse population (Cordes 2004).

Such an attempt could invest in more computationally-intensive *semi-coherent* dedispersion to limit intra-channel smearing and thus increase sensitivity (see, e.g., CDMT code and results, Bassa et al. 2017a,b; Maan et al. 2018).

5.4. Other future surveys and follow up

Given its large angular size – the LOFAR observations were almost 4° across – attempts to more deeply search M31 for transients are only possible with wide-field and/or high-survey-speed instruments.

Apertif, the successor to the system used by Braun et al. (2009) and Rubio-Herrera et al. (2013, cf. §3.1), can encompass M31 in a single pointing at 1.4 GHz, and has a powerful time-domain search backend (Oosterloo et al. 2009; van Leeuwen 2014; Maan & van Leeuwen 2017).

A 12-hr integration on M31 with MeerKAT, in the TRAPUM survey (Stappers & Kramer 2016), could detect periodic sources as dim as $2 \mu\text{Jy}$. If we follow the approach from Mikhailov & van Leeuwen (2016), and simulate one of our most luminous Galactic pulsars, B1641–45, with pseudo luminosity $L_r \geq 6 \text{ Jy kpc}^2$, in M31, it would appear as a $10 \mu\text{Jy}$ periodic source.

In single pulse searches of the kind we focused on in this paper, the Square Kilometre Array Mid can detect Crab-like pulsars from over a Mpc (Keane et al. 2015).

Arguably, though, the telescope most likely to find the first if not most pulsars in M31, is the Five hundred meter Aperture Spherical Telescope (FAST; Li & Pan 2016). At a sensitivity four times that of MeerKAT (Table 1, Dewdney et al. 2013), and other sources of interest outside of declination range, a deep campaign will prove profitable.

Our improved localisation of PSR J0044+4117 allows for follow up with narrow-field instruments. Such more sensitive single dishes may enable the identification of its periodicity and spin down.

6. Conclusions

We obtained some of the deepest pulsar search observations of Andromeda but did not detect any new pulsars. A hint of PSR J0044+4117 was seen in the 2011 observation but not confidently confirmed. We observed the Crab pulsar with the same LOFAR setup. We detected thousands of giant pulses, and measured the power-law index of the pulse-brightness probability density function to be 2.89 ± 0.02 . We extrapolate this distribu-

tion to the longer observation of, and larger distance to, M31. Any pulsar there that outshines the Crab by an order of magnitude, and whose single pulses are scattered the same way as FRBs, we would have detected. We conclude no such super-Crabs beamed at Earth exist in Andromeda.

Acknowledgements. We thank Marten van Kerkwijk for making available `digitize.py`, and Anya Bilous and Jean-Mathias Grießmeier for comments on the manuscript. The research leading to these results has received funding from the European Research Council under the European Union’s Seventh Framework Programme (FP/2007-2013) / ERC Grant Agreement n. 617199, and from the Netherlands Research School for Astronomy (NOVA4-ARTS). This paper is based on data obtained with the International LOFAR Telescope (ILT) under project codes `CODE_OF_L30906` and `CODE_OF_L246341`. LOFAR (van Haarlem et al. 2013) is the Low Frequency Array designed and constructed by ASTRON. It has observing, data processing, and data storage facilities in several countries, that are owned by various parties (each with their own funding sources), and that are collectively operated by the ILT foundation under a joint scientific policy. The ILT resources have benefitted from the following recent major funding sources: CNRS-INSU, Observatoire de Paris and Université d’Orléans, France; BMBF, MIWF-NRW, MPG, Germany; Science Foundation Ireland (SFI), Department of Business, Enterprise and Innovation (DBEI), Ireland; NWO, The Netherlands; The Science and Technology Facilities Council, UK; Ministry of Science and Higher Education, Poland. This work was carried out on the Dutch national e-infrastructure with the support of SURF Cooperative. Computing time was provided by NWO Physical Sciences (project №15310).

References

- Alexov, A., Hessels, J., Mol, J. D., Stappers, B., & van Leeuwen, J. 2010, in *Astronomical Society of the Pacific Conference Series*, Vol. 434, *Astronomical Data Analysis Software and Systems XIX*, ed. Y. Mizumoto, K.-I. Morita, & M. Ohishi, 193
- Bassa, C. G., Pleunis, Z., & Hessels, J. W. T. 2017a, *Astronomy and Computing*, 18, 40
- Bassa, C. G., Pleunis, Z., Hessels, J. W. T., et al. 2017b, *ApJL*, 846, L20
- Bhandari, S., Keane, E. F., Barr, E. D., et al. 2018, *MNRAS*, 475, 1427
- Bietenholz, M. F., Kassim, N., Frail, D. A., et al. 1997, *ApJ*, 490, 291
- Bilous, A. V., Kondratiev, V. I., Kramer, M., et al. 2016, *A&A*, 591, A134
- Braun, R., Thilker, D. A., Walterbos, R. A. M., & Corbelli, E. 2009, *ApJ*, 695, 937
- Chemin, L., Carignan, C., & Foster, T. 2009, *ApJ*, 705, 1395
- CHIME/FRB Collaboration, Amiri, M., Bandura, K., et al. 2019, *Nature*, 566, 230
- Chomiuk, L., & Povich, M. S. 2011, *AJ*, 142, 197
- Coenen, T., van Leeuwen, J., Hessels, J. W. T., et al. 2014, *A&A*, 570, A60
- Cordes, J. M. 2004, in *Astronomical Society of the Pacific Conference Series*, Vol. 317, *Milky Way Surveys: The Structure and Evolution of our Galaxy*, ed. D. Clemens, R. Shah, & T. Brainerd, 211
- Cordes, J. M., & Wasserman, I. 2016, *MNRAS*, 457, 232
- Cordes, J. M., Wharton, R. S., Spitler, L. G., Chatterjee, S., & Wasserman, I. 2016, *ArXiv e-prints*
- Deller, A. T., Goss, W. M., Brisken, W. F., et al. 2019, *ApJ*, 875, 100
- Dewdney, P. E., Turner, W., Millenaar, R., et al. 2013, http://www.skatelescope.org/wp-content/uploads/2013/03/SKA-TEL-SKO-DD-001-1_BaselineDesign1.pdf
- Eposito, P., Israel, G. L., Belfiore, A., et al. 2016, *MNRAS*, 457, L5
- Green, D. A. 2014, *Bulletin of the Astronomical Society of India*, 42, 47
- Haslam, C. G. T., Salter, C. J., Stoffel, H., & Wilson, W. E. 1982, *A&AS*, 47, 1
- Hewish, A., Bell, S. J., Pilkington, J. D. H., Scott, P. F., & Collins, R. A. 1968, *Nature*, 217, 709
- Karuppusamy, R., Stappers, B. W., & Lee, K. J. 2012, *A&A*, 538, A7
- Keane, E., Bhattacharyya, B., Kramer, M., et al. 2015, *Advancing Astrophysics with the Square Kilometre Array (AASKA14)*, 40
- Keane, E. F., & Kramer, M. 2008, *MNRAS*, 391, 2009
- Kondratiev, V. I., Verbiest, J. P. W., Hessels, J. W. T., et al. 2016, *A&A*, 585, A128
- Lee, J. H., & Lee, M. G. 2014, *ApJ*, 786, 130
- Li, D., & Pan, Z. 2016, *Radio Science*, 51, 1060
- Lyon, R. J., Stappers, B. W., Cooper, S., Brooke, J. M., & Knowles, J. D. 2016, *MNRAS*, 459, [arXiv:1603.05166 \[astro-ph.IM\]](https://arxiv.org/abs/1603.05166)
- Maan, Y., Bassa, C., van Leeuwen, J., Krishnakumar, M. A., & Joshi, B. C. 2018, *ApJ*, 864, 16
- Maan, Y., & van Leeuwen, J. 2017, *ArXiv e-prints*
- McConnachie, A. W., Irwin, M. J., Ferguson, A. M. N., et al. 2005, *MNRAS*, 356, 979

- McConnell, D., McCulloch, P. M., Hamilton, P. A., et al. 1991, *MNRAS*, 249, 654
- McLaughlin, M. A., & Cordes, J. M. 2003, *ApJ*, 596, 982
- Michilli, D., Hessels, J. W. T., Lyon, R. J., et al. 2018, *MNRAS*, 480, 3457
- Mikhailov, K. 2018, PhD thesis, University of Amsterdam, Ch. 4, <http://hdl.handle.net/11245.1/d3a5406f-eb36-4bb8-a280-54a3eedd0a52>
- Mikhailov, K., & van Leeuwen, J. 2016, *A&A*, 593, A21
- Oosterloo, T., Verheijen, M. A. W., van Cappellen, W., et al. 2009, in *Wide Field Astronomy & Technology for the Square Kilometre Array*, 70
- Ovidius, P. N. 8, in *Metamorphoses*, ed. A. Golding (London: W. Seres)
- Pastor-Marazuela, I., Webb, N. A., Wojtowicz, D., & van Leeuwen, J. 2019, *A&A*, *submitted*
- Ransom, S. M. 2001, PhD thesis, Harvard University
- Ravi, V., Shannon, R. M., & Jameson, A. 2015, *ApJ*, 799, L5
- Renting, G. A., & Holties, H. A. 2011, in *Astronomical Society of the Pacific Conference Series*, Vol. 442, *Astronomical Data Analysis Software and Systems XX*, ed. I. N. Evans, A. Accomazzi, D. J. Mink, & A. H. Rots, 49
- Rodríguez Castillo, G. A., Israel, G. L., Esposito, P., et al. 2018, *ApJ*, 861, L26
- Rubio-Herrera, E., Stappers, B. W., Hessels, J. W. T., & Braun, R. 2013, *MNRAS*, 428, 2857
- Sallmen, S., Backer, D. C., Hankins, T. H., Moffett, D., & Lundgren, S. 1999, *ApJ*, 517, 460
- Sanidas, S., Cooper, S., Bassa, C. G., et al. 2019, *A&A*, 626, A104
- Stappers, B., & Kramer, M. 2016, in *Proceedings of MeerKAT Science: On the Pathway to the SKA*. 25-27 May, 9
- Stappers, B. W., Hessels, J. W. T., Alexov, A., et al. 2011, *A&A*, 530, A80
- Stiele, H., Pietsch, W., Haberl, F., et al. 2011, *A&A*, 534, A55
- Tendulkar, S. P., Bassa, C. G., Cordes, J. M., et al. 2017, *ApJ*, 834, L7
- van Haarlem, M. P., Wise, M. W., Gunst, A. W., et al. 2013, *A&A*, 556, A2
- van Leeuwen, J. 2014, in *The Third Hot-wiring the Transient Universe Workshop*, ed. P. R. Wozniak, M. J. Graham, A. A. Mahabal, & R. Seaman, 79
- van Leeuwen, J., & Stappers, B. W. 2010, *A&A*, 509, A7
- Williams, B. F. 2003, *AJ*, 126, 1312
- Yao, J. M., Manchester, R. N., & Wang, N. 2017, *ApJ*, 835, 29
- Yin, J., Hou, J. L., Prantzos, N., et al. 2009, *A&A*, 505, 497

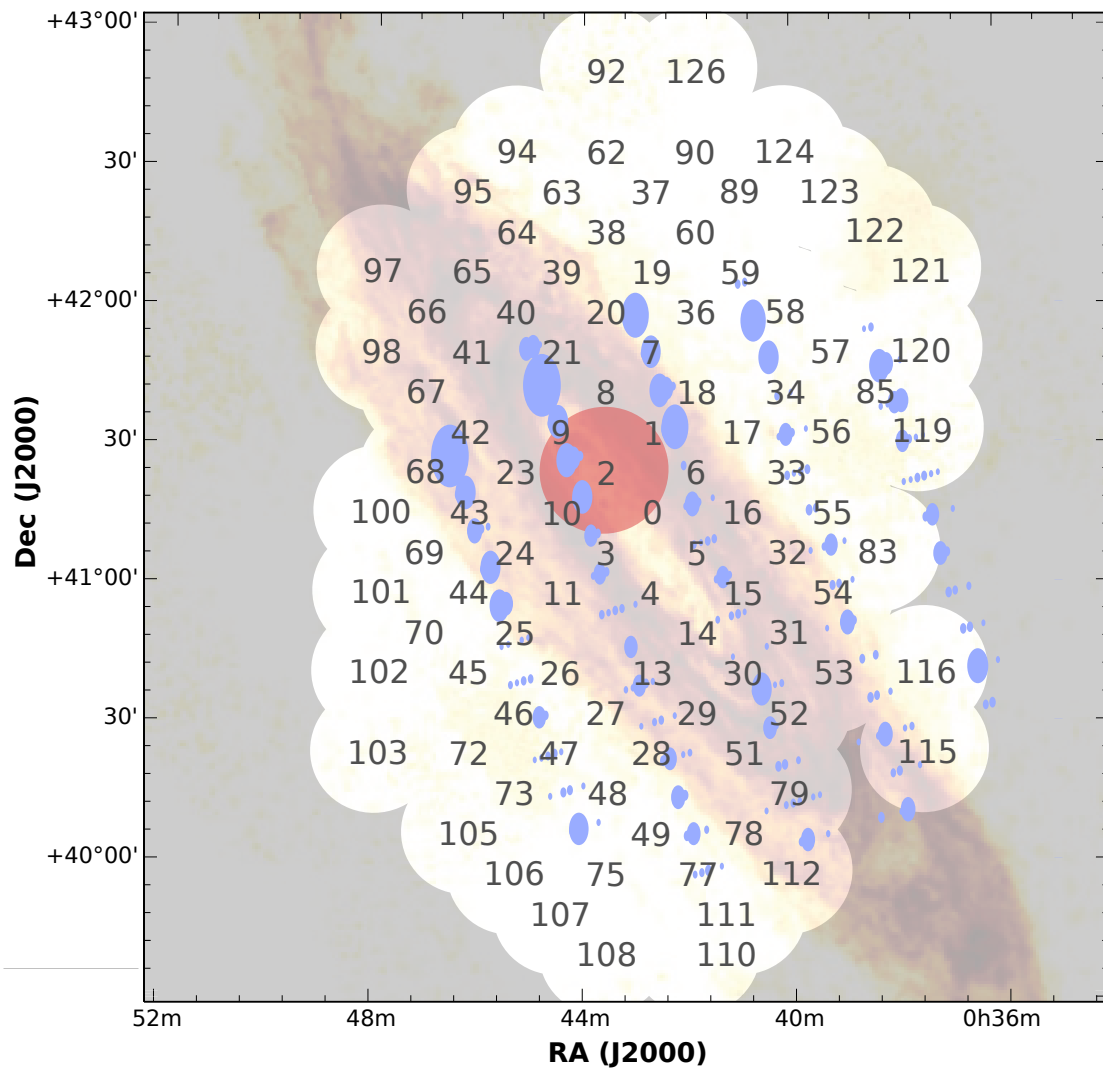


Fig. 1: The union of our 2011 beam pattern with the localization distribution of the $DM = 54.7 \text{ pc cm}^{-3}$ candidate from [Rubio-Herrera et al. \(2013\)](#) in blue. The overall outline and beam numbers over the 2011 observation are shown; the 25 absent beams failed initial processing. As observations were taken around transit, the beams are close to circular. The size of the blue ellipses indicates the S/N of the single-pulse detection in that WSRT subbeam. In red, the LOFAR beam in which the pulsar was detected. In the background, the H I peak brightness map at 60 arcsec and 6 km s^{-1} resolution, as observed with Westerbork Synthesis Radio Telescope ([Braun et al. 2009](#)). The 91 tied-array beams pattern from 2014 overlaid on a 10-hr LOFAR imaging observation of M31 is found in [Mikhailov \(2018\)](#).

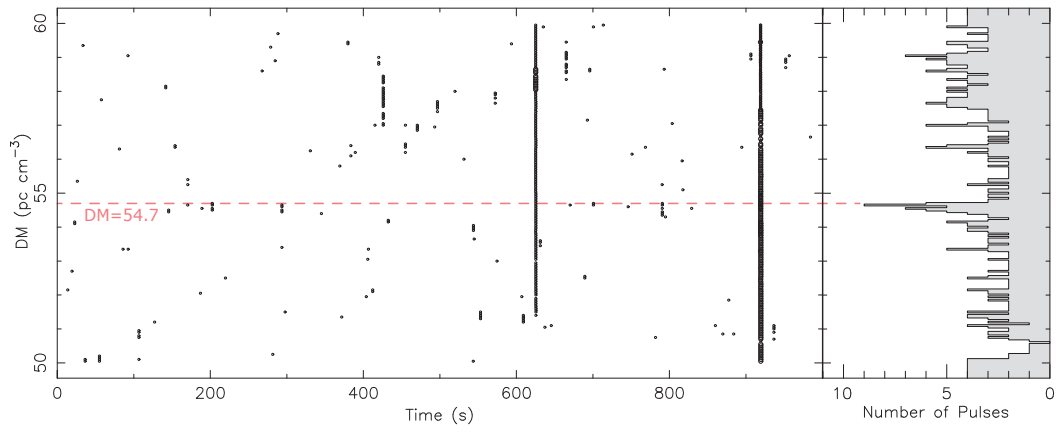


Fig. 2: The 2011 data for Beam 2. In the left panel, 8 weak single pulses can be identified. In the right panel, the resulting excess at $DM = 54.7 \text{ pc cm}^{-3}$ is seen in the candidate histogram.

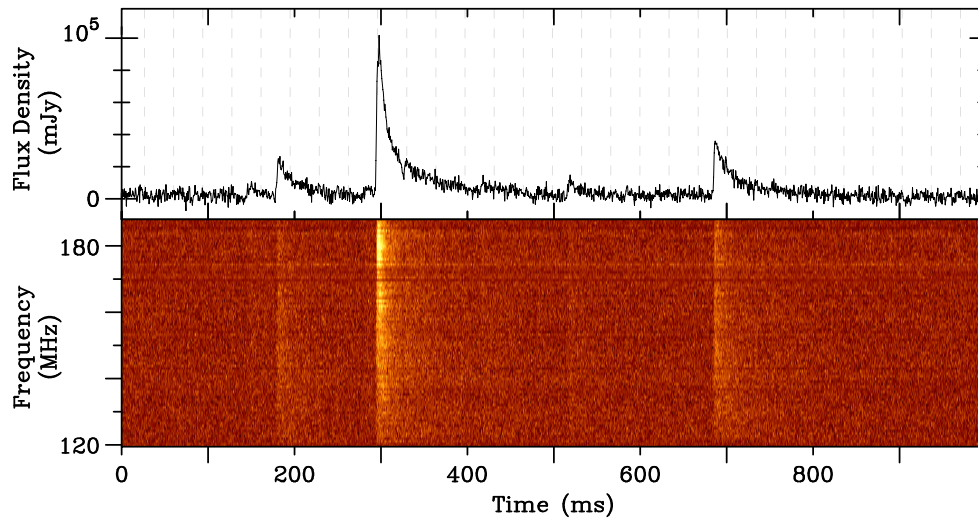


Fig. 3: One second of LOFAR data containing multiple giant pulses. Dashed lines indicate the same phase as the onset of the highest pulse. Giant pulses occur at both main and inter pulse phase.

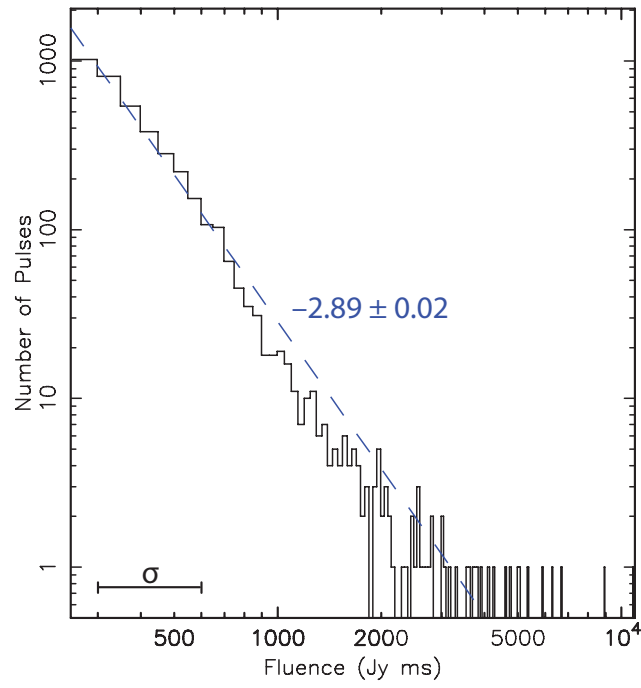


Fig. 4: The Crab fluence distribution from 1 hr of LOFAR data in the same setup as the M31 search, plus the power-law best fit. The measurement error σ on the fluence values is indicated bottom-left.

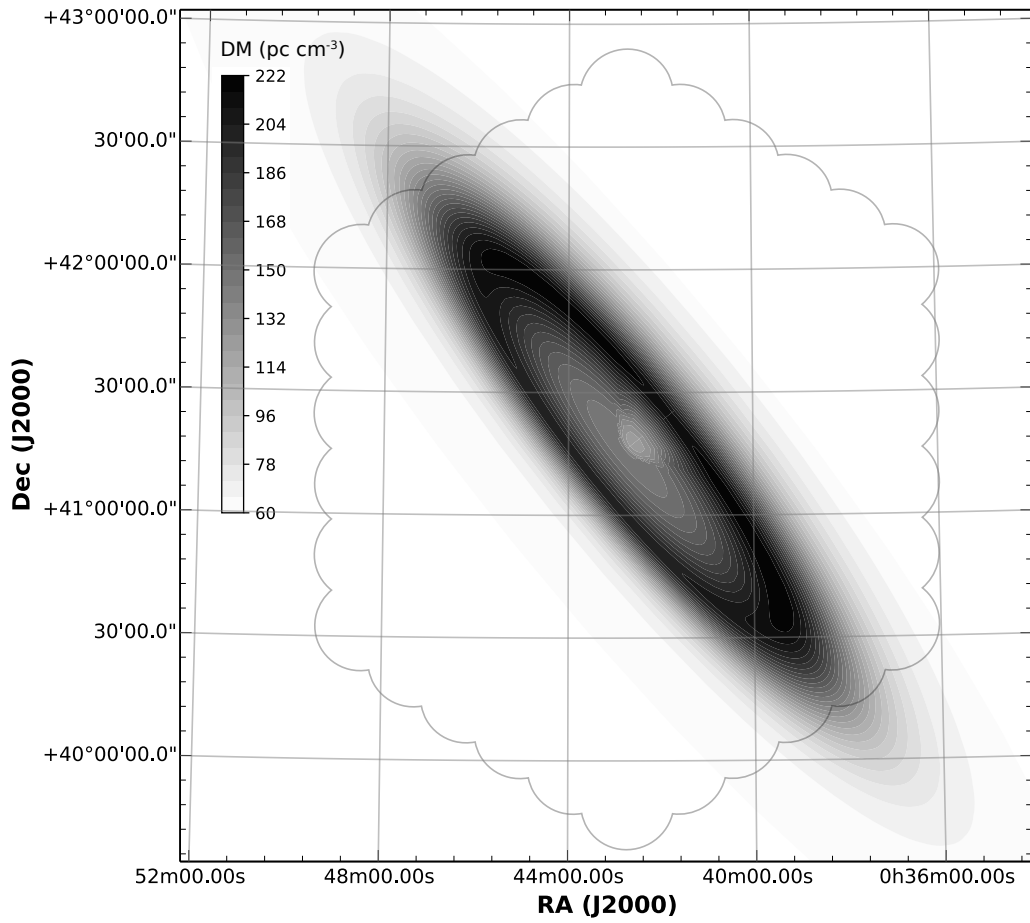


Fig. 5: Expected total dispersion measure for sources in the mid plane of M31. The galactic foreground is seen throughout. The 91 tied-array beams pattern from 2014 shown in outline.